Topology Preserving Deformable Image Matching Using Constrained Hierarchical Parametric Models

Oliver Musse, Fabrice Heitz, and Jean-Paul Armspach

Abstract—In this paper, we address the issue of topology preservation in deformable image matching. A novel constrained hierarchical parametric approach is presented, that ensures that the mapping is globally one-to-one and thus preserves topology in the deformed image. The transformation between the source and target images is parameterized at different scales, using a decomposition of the deformation vector field over a sequence of nested (multiresolution) subspaces. The Jacobian of the mapping is controlled over the continuous domain of the transformation, ensuring actual topology preservation on the whole image support. The resulting fast nonlinear constrained optimization algorithm enables to track large nonlinear deformations while preserving the topology. Experimental results are presented both on simulated data and on real medical images.

Index Terms—Deformable image matching, hierarchical parametric models, multiresolution deformation field modeling, topology preservation.

I. INTRODUCTION

IMAGE matching of deformable structures has received considerable attention during the last decade [1]. Medical imaging, revealing anatomical structures using a wide variety of sensors, is probably one of the first application fields. A key research topic is inter-subject or atlas-subject registration, where the purpose is to estimate long-distance and highly nonlinear deformations corresponding to anatomical variability between individuals. Potential applications include image segmentation and labeling [2], [3], atlas-based multimodal image registration or fusion [4], motion analysis in three-dimensional (3-D) image sequences [3], statistical analysis of normal and pathological anatomical variations [5]–[7], atlas-based follow-up of lesion evolution over time [8], and atlas-based volume estimation [9], [10].

The high dimensional transformations involved in deformable registration generally make the problem ill-conditioned, so that additional constraints are needed to obtain a satisfactory result. A common way to do this is to restrict the space of possible solutions by incorporating *a priori* knowledge in the deformation model. Standard regularization techniques [11] such as Laplacian [12], bending energy [13], or linear elasticity [2], are a popular choice. A regularizing potential energy, constraining the deformation, is minimized simultaneously

with a cost function describing image differences. Often, this is handled through a Bayesian framework [14], where constraints are incorporated into the warping model as prior probability distributions. Fast regularization methods have also been proposed, relying on an iterative filtering of the discrete vector field with a Gaussian [3]. Others have investigated parametric transformations using, for instance, polynomial spline [5], [15], thin-plate spline [16] or wavelets [17], so that the constraints are explicitly included in a parametric deformation model.

In most of these approaches, the prior enforces homogeneity of the deformation field through linear regularization models. This is related to the "smoothness" of the deformation and proved to be efficient in many applications when addressing small deformations problems. The problem is significantly harder for large nonlinear deformations. Since the constraint generally increases proportionally to the deformation magnitude, it becomes difficult to simultaneously estimate a regular and satisfactory transformation, even when using coarse to fine strategies. Furthermore, standard regularization methods do not preserve the topology in the deformed images.

Topology preservation is a stronger and global constraint, ensuring that connected structures remain connected and that the neighborhood relationship between structures is maintained. It also prevents the disappearance or appearance of existing or new structures. These properties are related to the continuity and inversibility of the deformation. Topology-preserving matching is particularly interesting for inter-subject registration of medical images, since, in the continuous domain, anatomical structures have the same topology for any individual (at least for nonpathological cases). By enforcing this constraint, the space of possible solutions is restricted to deformations satisfying the real-world property of matter. In particular, it represents a challenging issue for the construction and use of anatomical atlases. For instance, when labeling a template by transferring atlas knowledge through mapping, it is essential to ensure topology preservation of the atlas structures to get an anatomically coherent solution.

Topology-preserving mapping has already been considered with success in a few works. In [18], Christensen introduced viscous fluid material deformation models, in an Eulerian framework, by using the Navier–Stokes partial derivative equations (PDEs). This allows large displacement estimation compared to elastic Lagrangian approaches, while ensuring topology preservation. An interesting discussion on the topological properties of this model can be found in [19]. Important drawbacks are the computational cost and the necessity to track the discrete Jacobian in order to avoid numerical divergence when solving the PDE. In [20], Trouvé restricted the space of solutions to a subgroup of invertible mappings by exploiting Lie group theory.

The problem was expressed as a regularization scheme or using PDE, shown to be linked to the fluid model of Christensen. The proposed numerical scheme was more stable so that no discrete Jacobian tracking was needed. Ashburner [21] solved the issue in a Bayesian framework, where the Gibbs potential associated to the prior distribution is a function of the Jacobian. By penalizing noninvertible solutions through low probabilities, the mapping is ensured to preserve almost surely the topology. Finally, some authors have addressed the topological issue by considering simultaneously backward and forward maps, constraining *a posteriori* the composite of both to reduce to identity [3]. Such an approach is fast and simple but does not mathematically ensure the preservation of the topology.

In this paper, we propose an alternative approach, based on a hierarchical continuous parametric model of the deformation map, described in [17]. The proposed topology preserving method allows to enforce the positivity of the Jacobian J of the continuous transformation, within a specified interval of values. Instead of expressing the topology preserving constraints through PDE or Bayesian approaches, the continuous deformation model is strictly constrained. We establish the possibility to control the positivity of the Jacobian over the whole (continuous) image domain, by applying only a limited (discrete) set of linear constraints on the parameters of the deformation model. An energy function describing the interactions between the two images is then minimized under this set of constraints, ensuring that the transformation maintains the topology in the deformed image. Thanks to the limited number of linear constraints and to the hierarchical modeling approach, the constrained optimization algorithm enables fast estimation of long range, nonlinear deformation fields (cpu times are about 1 min on a standard workstation for 256^2 images).

The remainder of the paper is organized as follows. Section II presents an overview of the mathematical issues related to topology preservation, in which the conditions needed to ensure topology preservation are recalled. In Section III, the multiresolution parametric matching method is briefly described. The extension of this model in order to preserve topology is then detailed in Section IV. Finally, results on both simulated and real-world data are discussed in Section V.

II. TOPOLOGY PRESERVING MAPPINGS

The purpose of deformable matching is to estimate the transformation between two different images (the source and the target) so that, after registration, the corresponding structures are superimposed in the target image and in the deformed version of the source image. Let us denote $h : \Omega \longrightarrow \Omega$ the continuous transformation, where Ω is the domain on which the images are defined. To be a topology-preserving mapping, h must be homeomorphic, which means that it must be (a) continuous, (b) bijective (one-to-one and onto) with (c) a continuous inverse. The continuity of the deformation is related to the local neighborhood relationship between structures, and maintains their adjacency, while global bijectivity ensures that each point in the source image has one and only one corresponding point in the target and conversely.

Even though the continuity and onto properties may be directly and easily imposed through the definition of the defor-

mation model (see Section IV-A), the other conditions are not straightforward. First, as stated in the following theorem [22], when working on a closed bounded set, the continuity condition (c) for the inverse transformation is a consequence of the other properties.

Theorem 1: Let T be a continuous transformation which is one-to-one in a closed bounded set S. Then, the corresponding inverse transformation T^{-1} is continuous, and maps $T(S)$ back onto S.

As a consequence, the major issue is now to ensure the global injectivity of h. A common solution consists of forcing the Jacobian of the deformation to be positive [22].

Theorem 2: Let T be a transformation from E^n into E^n (E^n is the space defined as the cross product $E \times E \times E \cdots \times E$ of n spaces E) which is of class C^1 in an open subset D of E^n, and suppose that the Jacobian $J(p) > 0$ for each $p \in D$. Then, T is locally one-to-one in D.

However, the positivity constraint on the Jacobian only ensures local injectivity of T, which means that for each point $p \in D$ there exists a neighborhood in which T is injective (or one-to-one). To infer global injectivity from local injectivity, additional conditions are needed (see [22]–[25]).

Theorem 3: Let $T : B \rightarrow B^*$ be a continuous locally one-to-one transformation. If B and B^* are convex then T is globally one-to-one.

From all these theorems, we can now state that if the mapping h is continuous, onto, and locally one-to-one over the convex set Ω and if $h(\Omega)$ is convex, then h is a global homeomorphism from Ω into $h(\Omega)$. To get a topology-preserving transformation from Ω into Ω and therefore enforce $h(\Omega) = \Omega$, a sufficient condition is to ensure that h maps the boundary of Ω exactly onto itself. Under this additional condition, the convexity of $h(\Omega)$ directly derives from the convexity of Ω. As a consequence, it finally follows that if h is a **continuous, onto, locally injective** transformation over the **convex set** Ω and if h **maps exactly the boundary of** Ω **on itself**, then h is a **topology-preserving mapping from** Ω **into** Ω. These properties will be exploited, to ensure topology preservation over the whole (continuous) domain Ω, in the case of the hierarchical parametric deformation model described now.

III. HIERARCHICAL DEFORMABLE IMAGE MATCHING

In [17], we have introduced a hierarchical parametric modeling framework to perform fast nonrigid image matching. The present work is based on an extension of the model and algorithms described in [17]. In particular, the optimization algorithms have been modified to increase their efficiency (by exploiting the local decomposition properties of the model) and to take into account topology preservation. Before detailing this extension, the following section provides the basis of our hierarchical deformable matching approach. For greater detail and more results about the method, the reader is referred to [17].

A. General Approach

The deformable matching method uses the common framework [18], [20] of estimating a displacement field **u**, by min-

imizing the following nonlinear distance measure (or energy function) E between the target image and the source image

$$E(\mathbf{u}) = \int_\Omega |I_1(s) - I_2(s + \mathbf{u}(s))|^2 ds \tag{1}$$

where
- Ω bounded domain defined by the images;
- I_2 floating (source) image to be mapped onto the target image I_1;
- s pixel position over Ω.

$\mathbf{u}$, denoting the deformation vector field, belongs to an adequate Hilbert space $\mathcal{H}$ of finite energy deformation fields. The continuous mapping h between the two images is then defined as

$$h(s) = s + \mathbf{u}(s). \tag{2}$$

Instead of estimating directly the vector field $\mathbf{u}$ within $\mathcal{H}$, successive approximations of $\mathbf{u}$ are considered over a sequence of nested subspaces of the original configuration space $\mathcal{H}$. This sequence of subspaces defines a sequence of multiresolution approximations [26] of vector field $\mathbf{u}$, as explained below.

B. Deformation Model

The transformation between the two images is parameterized at different scales, using a decomposition of the deformation vector field $\mathbf{u}$ over a sequence of nested subspaces $V_0 \subset V_1 \subset \cdots \subset V_l \subset V_{l+1} \subset \cdots \subset \mathcal{H}$, defining a multiresolution approximation of $\mathbf{u}$ [26]. Space V_0 defines the coarsest scale representation and is a subset of the finer scale representations $V_1 \subset \cdots V_l \subset \cdots$. Mallat [26], [27] has shown that nonorthogonal (Riesz) basis of these spaces may be generated from dilated and translated versions of a single compactly supported scaling function ϕ [27].[1] In one dimension, a Riesz basis of V_l is constructed by the set of functions ϕ_i^l

$$\phi_i^l = 2^{l/2}\phi(2^l x - i). \tag{3}$$

To represent two-dimensional (2-D) signals, a separable scaling function $\phi_{2D}(x, y) = \phi(x)\phi(y)$ is considered, so that the Riesz basis of V_l becomes

$$\phi_{i,j}^l = 2^l \phi_{2D}(2^l x - i, 2^l y - j) = 2^l \phi(2^l x - i)\phi(2^l y - j). \tag{4}$$

Then, in order to handle a deformation field (i.e., to modelize vectors instead of scalars), two multiresolution decompositions are considered, one for each component of the displacement. At resolution l (in space V_l) the parameterization of $\mathbf{u}$ is therefore defined as

$$\mathbf{u}^l(x, y) = \begin{cases} u_x^l(x, y) = \sum_{i=0}^n \sum_{j=0}^n a_{x_{i,j}}^l \phi_{i,j}^l(x, y) \\ \qquad = \text{trace}\left(A_x^{l^{\mathrm{T}}} \Phi^l\right) \\ u_y^l(x, y) = \sum_{i=0}^n \sum_{j=0}^n a_{y_{i,j}}^l \phi_{i,j}^l(x, y) \\ \qquad = \text{trace}\left(A_y^{l^{\mathrm{T}}} \Phi^l\right) \end{cases} \tag{5}$$

---

[1]To define a Riesz basis, function ϕ must verify some technical conditions, which may be found in [27].
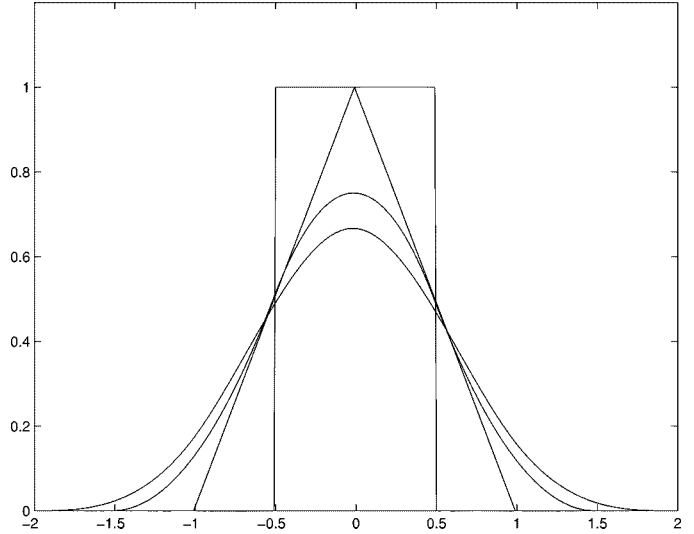

Fig. 1.   Polynomial spline scaling functions ϕ_d (6) for $d = 0, 1, 2$, and 3.

where $\Phi^l = (\phi_{i,j}^l)_{i,j=0,...,n}$ is a matrix formed with the basis functions of V_l and $A_x^l = (a_{x_{i,j}}^l)_{i,j=0,...,n}$ and $A_y^l = (a_{y_{i,j}}^l)_{i,j=0,...,n}$ are the matrices of parameters for each component of the deformation vector. Note that the sum is limited to $i = 0, \ldots, n$ and $j = 0, \ldots, n$ where $n = 2^l - b_\phi$ and b_ϕ is the size of the support of the scaling function ϕ. Indeed, since Ω is a bounded set and ϕ is compactly supported, we only consider the basis functions, the support of which is partly included in Ω.

In the remainder of the paper, $\mathbf{u}$ (resp. $h(s) = s + \mathbf{u}(s)$) will denote the deformation field (resp. transformation) in general, for example, to express the conditions it should satisfy to ensure topology preservation and $\mathbf{u}^l$ (resp. $h^l(s) = s + \mathbf{u}^l(s)$) will denote the parametric deformation field (resp. transformation) at resolution 2^l, this notation being used as soon as the considerations are specific to the parametric model.

The hierarchical parametric representation (5) is valid for any scaling function ϕ defining a Riesz basis. For this implementation, we have used a nonorthogonal Riesz basis of polynomial splines, constructed with *box splines* [27]. The variable order polynomial spline functions (Fig. 1) are defined as follows:

$$\phi_0(x) = \begin{cases} 1, & \text{for } x \in \left[-\frac{1}{2}, \frac{1}{2}\right[\\ 0, & \text{otherwise} \end{cases}$$
$$\phi_d(x) = \phi_0 * \phi_{d-1}(x) \tag{6}$$

where d denotes the order of the representation. $d = 0$ corresponds to the classical piecewise constant Haar basis. $d = 1$ defines continuous and piecewise linear functions in 1-D (but a nonlinear representation for the 2-D separable case). These functions have the advantage of being explicitly defined and compactly supported. Nonorthogonal representations have been preferred to orthogonalized Riesz bases because the resulting orthogonal bases have infinite support [27].[2]

Another interest of this model, which derives directly from the causality property $V_l \subset V_{l+1}$, is that the approximation of the deformation at resolution l may be expanded over the finer

---

[2]Orthogonality is not important in our case, since we are modeling an unknown signal rather than analysing a known signal.
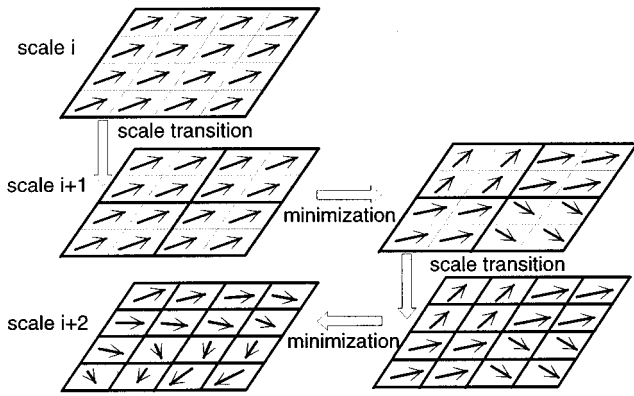
Fig. 2.   Hierarchical optimization procedure in the case of the 2-D Haar basis.

resolution space V_{l+1} *without any interpolation nor approximation*. It can be shown that the parameter matrices A_x^{l+1} and A_y^{l+1} of the decomposition over V_{l+1}, are simply derived from A_x^l and A_y^l, according to [26]

$$A_x^{l+1} = \left(\uparrow_2 \left(A_x^l\right)\right) * H \quad A_y^{l+1} = \left(\uparrow_2 \left(A_y^l\right)\right) * H \quad (7)$$

where $\uparrow_2$ is an operator which puts one zero between each element of a matrix, and H is a numerical convolution filter depending on the scaling function ϕ [26].

C. Matching Procedure

1) Hierarchical Optimization Strategy: In order to make use of the previously defined hierarchical decomposition, instead of minimizing the original energy function (1) over the full, continuous Hilbert space $\mathcal{H}$, we consider a coarse-to-fine sequence of optimization problems, obtained by successively restricting the vector field to subspaces $V_0, V_1, \ldots, V_L$ [28]. The energy function E (1) is minimized over each space $V_l, l = 0, \ldots, L$ with respect to parameters $A = (A_x^l, A_y^l)$, using as an initialization the estimation obtained at the previous scale. The tracking of the solution between two successive scales l and $l + 1$ is performed, without any interpolation (thanks to the causality property), using (7). The procedure is repeated until the desired scale L is reached, this scale being a compromise between the computational cost, the desired resolution, and the desired regularization of the vector field. As shown in [28], this hierarchical coarse-to-fine procedure exhibits fast convergence properties when applied to high-dimensional nonlinear optimization problems (with many local minima). Indeed, the energy function becomes *smoother* at coarse scales, and thus local deterministic optimization algorithms may be used to track the solution from coarse to fine scales.

Fig. 2 illustrates the algorithm for the ϕ_0 scaling function (corresponding to the Haar basis). The Haar basis representation amounts to constraining the deformation field to be blockwise constant over cells of decreasing size. The Haar basis is not used in the present application since it does not yield a continuous deformation, as required (see Section IV-A).

2) Separable Minimization Procedure: At each scale l, the energy function E (1) is minimized, as a function of the model parameters $A^l = (A_x^l, A_y^l)$. To this end, the local representation of the deformation and the possible decomposition of the energy

E (1) are exploited. Since the scaling function ϕ is compactly supported, the model parameters $a_{x_{i,j}}^l$ and $a_{y_{i,j}}^l$, associated to the basis function $\phi_{i,j}^l$, have a local impact on the deformation field $\mathbf{u}^l$. Instead of considering the simultaneous optimization of all the parameters A^l, the matching is performed by iteratively solving a sequence of local subproblems

> **loop**
>   **for** $(i, j) \in \{0, \ldots, n\}^2$
>   **Minimize** $E\left(a_{xi,j}^l, a_{yi,j}^l\right)$
> $$= \int_{\Omega_{i,j}^l} \left|I_1(s) - I_2(s + \mathbf{u}^l(s))\right|^2 ds$$
>   **end for** (i, j)
>   **until convergence** $\qquad\qquad\qquad\qquad (8)$

where $\Omega_{i,j}^l$ is the support of the basis function $\phi_{i,j}^l$.

This scheme is akin to the classical Gauss–Seidel optimization method which consists of minimizing in turn the objective function along all the directions of the parameters space, using a one-dimensional (1-D) minimization technique. Here, instead of considering one parameter at the same time, the two parameters $a_{x_{i,j}}^l$ and $a_{y_{i,j}}^l$ are estimated simultaneously. The optimization procedure is described in detail in Appendix D. This local minimization scheme significantly decreases the computational time (the number of parameters reaches 32 258 at the resolution level $L = 7$).

IV. TOPOLOGY PRESERVING HIERARCHICAL DEFORMABLE MATCHING

The hierarchical parametric mapping introduced in the previous section is *not* topology preserving, since, as may easily be verified, the Jacobian of the transformation may take negative values over domain Ω. In this section, we describe an extension of the matching procedure, which ensures topology preservation over the whole (continuous) domain Ω. Using the general results on topology preserving mappings (see Section II), we show that topology preserving constraints may easily be expressed through a limited set of linear inequalities on the deformation model parameters. A fast constrained minimization algorithm, relying on these constraints, is then devised.

A. Continuity and Boundary Conditions

The continuity of transformation $h^l(s) = s + \mathbf{u}^l(s)$, is ensured by using the general properties of the parametric model. Since, $\mathbf{u}^l$ is expressed as a linear combination of basis functions derived from a single scaling function ϕ (5) and (4), $\mathbf{u}^l$, and h^l inherit the continuity and differentiability properties of ϕ. As a consequence, the continuity of transformation h^l is simply obtained, by considering a continuous function ϕ. For the polynomial spline functions ϕ_d (6), this property is satisfied for $d \geq 1$.

To ensure that $h^l(\Omega) = \Omega$, the transformation must satisfy some Dirichlet boundary conditions corresponding to the nullity of $\mathbf{u}^l$ on the boundary $\delta\Omega$ of Ω. To this end, only the basis functions $\phi_{i,j}^l$ that have their support entirely included in Ω are retained. This principle is illustrated in Fig. 3, for the 1-D case and a degree 1 polynomial spline function ϕ_1.
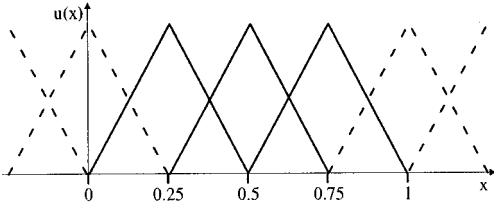
Fig. 3. Deformation field $\mathbf{u}^l$ is enforced to be null on the boundary of Ω by considering only the basis functions, the support of which is entirely included in Ω. In this figure, the 1D case ($\Omega = [0, 1]$) and the polynomial spline function of degree 1 are considered. The basis functions represented with solid lines are kept, while those represented with dashed lines are excluded from the model.

B. Local One-to-One Property

As stated in Section II, topology preservation requires local injectivity of the deformation, which, under the right conditions, may lead to global injectivity. According to Theorem 2 (Section II), for a C^1 transformation, local injectivity is obtained by enforcing the Jacobian $J_h(s)$ to be positive for each point $s \in \Omega$, where $J_h(s)$ is the Jacobian of h at point $s \in \Omega$. Taking advantage of the local minimization scheme presented in (8), and ensuring the adequate boundary conditions, as explained in Section IV-A, a topology preserving version of the matching method may thus be expressed as

$$\forall (i,j) \in \{0, 1, \dots, n\}^2$$
$$\textbf{Minimize } E\left(a_{x_{i,j}}^l, a_{y_{i,j}}^l\right)$$
$$= \int_{\Omega_{i,j}^l} \left| I_1(s) - I_2(s + \mathbf{u}^l(s)) \right|^2 ds$$
$$\textbf{subject to } \forall (x,y) \in \Omega_{i,j}^l \quad J_{h^l}(x,y) > 0. \tag{9}$$

This constrained minimization is performed while keeping the hierarchical strategy introduced in Section III-C.I. In each space V_l, the solution obtained at the previous scale is tracked and used as an initialization. According to the causality property $V_l \subset V_{l+1}$, each scale transition step preserves the deformation field $\mathbf{u}^l$ so that the positivity property $\forall s \in \Omega \; J_{h^l}(s) > 0$ is also propagated through the scale spaces. The hierarchical strategy and the constrained minimization are therefore associated in a mathematical coherent way.

The principal issue thus consists in ensuring condition $J_{h^l}(s) > 0$ for all the points in $\Omega_{i,j}^l$. The Jacobian J_{h^l} may be easily expressed as a function of the scaling function ϕ and of the model parameters. In Appendix A, it is shown that, for any scaling function ϕ, J_{h^l} is linear with respect to parameters $a_{x_{i,j}}^l$ and $a_{y_{i,j}}^l$. As a consequence, the positivity constraint on the Jacobian may be expressed as a set of **linear** inequalities on the model parameters. This is an appealing feature, since linear inequalities are easily handled in constrained minimization methods. The number of inequalities to be considered is however equal to the number of points in $\Omega_{i,j}^l$. For a control of positivity over the whole continuous domain, this yields an infinite set of constraints. A solution often used in other approaches, is to compute the Jacobian (or finite difference approximations of the Jacobian) on the discrete image lattice only. The set of constraints is then reduced to the number of pixels in $\Omega_{i,j}^l$. However, this approach does not ensure Jacobian positivity for all points on the continuous domain Ω, so that

topology preservation can no longer be guaranteed by the theorems in Section II, which are valid only for continuous transformations. The method proposed in this paper enforces local injectivity over the whole continuous domain $\Omega_{i,j}^l$ and not only on the discrete lattice, as explained now.

To overcome this key problem, we have considered the degree 1 polynomial spline scaling function ϕ_1. By using this scaling function, we show that the Jacobian $J_{h^l}(x,y)$ is piecewise linear with respect to x and y (see Appendix B). More precisely, at resolution 2^l, J_{h^l} is linear with respect to x and y over each square domain $S_{k,m}^l = [k/2^l, (k+1)/2^l] \times [m/2^l, (m+1)/2^l]$, $k = 0, \dots, 2^l - 1$, $m = 0, \dots, 2^l - 1$. To enforce Jacobian positivity over domain $S_{k,m}^l$, it is therefore sufficient to impose this condition at the four corners of $S_{k,m}^l$, which corresponds to only four linear inequality constraints. The support $\Omega_{i,j}^l$ being the union of the four square domains $S_{i,j}^l$, $S_{i+1,j}^l$, $S_{i,j+1}^l$, and $S_{i+1,j+1}^l$, the condition $\forall (x,y) \in \Omega_{i,j}^l$, $J_{h^l}(x,y) > 0$ is easily obtained with a set of only 16 inequality constraints. The matching procedure then becomes

$$\forall (i,j) \in \{0, 1, \dots, n\}^2$$
$$\textbf{Minimize } E\left(a_{x_{i,j}}^l, a_{y_{i,j}}^l\right)$$
$$= \int_{\Omega_{i,j}^l} \left| I_1(s) - I_2(s + \mathbf{u}^l(s)) \right|^2 ds$$
$$\textbf{subject to } M_{i,j}^l \begin{pmatrix} a_{x_{i,j}}^l \\ a_{y_{i,j}}^l \end{pmatrix} + b_{i,j}^l > 0 \tag{10}$$

where $M_{i,j}^l$ and $b_{i,j}^l$ are, respectively, a matrix and a vector related to the 16 necessary and sufficient control points over $\Omega_{i,j}^l$ (the expressions of $M_{i,j}^l$ and $b_{i,j}^l$ are given in Appendix B).

A final problem comes from the strong assumption of Theorem 2, that h should be a C^1 transformation. With the ϕ_1 scaling function, this assumption is not verified: h^l is only piecewise C^1. As a consequence, local injectivity cannot be directly inferred from Theorem 2. Fortunately, the property still holds in our case: an extension of Theorem 2 is demonstrated in Appendix C.

Practically, the constrained optimization problem (10) may be addressed with any existing approach, using the linearity of the constraint [29], [30]. For our implementation, we have developed a fast method, close to sequential linear programming [30]. The algorithm is described in Appendix D.

Finally, let us notice that, beside topology preservation, the Jacobian is also related to the compression and dilation properties of matter. In some applications, it might be interesting to enforce the Jacobian between user-defined values $0 < J_{\min} \leq J_h \leq J_{\max}$. This may be achieved with few modifications of the method. The number of inequality constraints is simply increased to 32 (16 for each inequality)

$$\forall (i,j) \in \{0, 1, \dots, n\}^2$$
$$\textbf{Minimize } E\left(a_{x_{i,j}}^l, a_{y_{i,j}}^l\right)$$
$$= \int_{\Omega_{i,j}^l} \left| I_1(s) - I_2(s + \mathbf{u}^l(s)) \right|^2 ds$$
$$\textbf{subject to } 0 < J_{\min} < M_{i,j}^l \begin{pmatrix} a_{x_{i,j}}^l \\ a_{y_{i,j}}^l \end{pmatrix} + b_{i,j}^l J_{\max}. \tag{11}$$
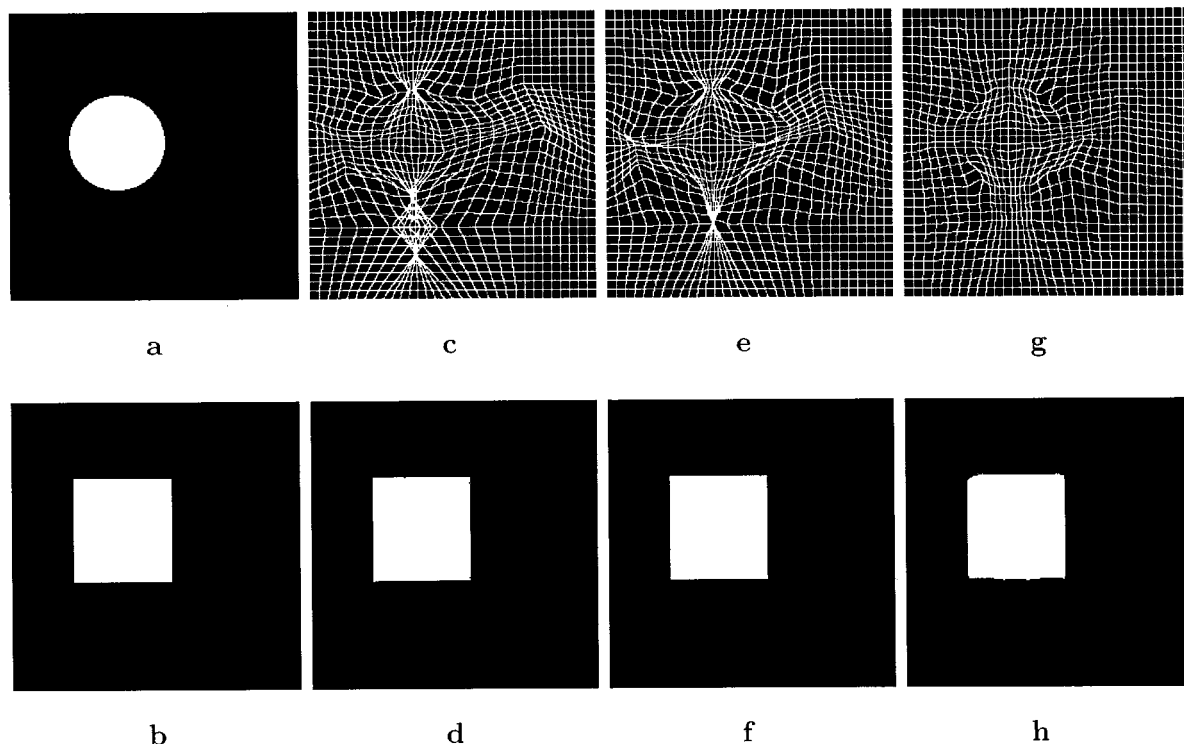
Fig. 4.   Deformable matching of (a) a circle on (b) a square. For each method, the transformation is applied to a regular grid of lines, to visualize the underlying deformation field. Deformable matching is performed: (c) and (d) without any constraint; (e) and (f) with a positivity constraint $J > 0$; and (g) and (h) with the constraint $J > 0.5$.

V. RESULTS

To illustrate the contribution of topology preservation, we first present an example showing the mapping of two simple binary shapes [a circle and a square, as shown in Fig. 4(a) and (b)]. The deformation field that maps the circle on the square is nonlinear and long-range (in the sense that it may not be estimated with local differential methods [31], [32]). Fig. 4(d)–(h) displays the deformed images of the circle, obtained with different constraints. We simultaneously apply the same transformations to a regular grid, to visualize the underlying deformation field [Fig. 4(c)–(g)]. As expected, the unconstrained deformable matching method [Fig. 4(c) and (d)] does not preserve topology and yields singularities in the deformation field, which may be detrimental in most applications. These singularities appear clearly as folds or line crossings on the deformed grid [Fig. 4(c)]. This is not the case for the constrained matching algorithm, which clearly ensures the bijectivity of the transformation [see Fig. 4(e) and (f)], while providing a satisfactory mapping. This shows that, in the space of possible solutions that warp the circle onto the square, the constrained method is able to retrieve a topology preserving transformation. On the other hand, when the minimal value of the Jacobian is unduly increased ($J \geq 0.5$), the deformation field becomes smoother, but is unable to match exactly the target shape [see Fig. 4(g) and (h)].

In the previous example, the singularities in the unconstrained approach are only visible on the regular grid and have no consequences on the appearance of the resulting deformed shape [Fig. 4(c) and (d)]. In Fig. 5, we show a second, more

involved example, with larger, nonlinear deformations. This example is somewhat beyond the representation capabilities of our model, since it is not possible to obtain an exact match in this case. Fluid deformation models [18], [20] are necessary to cope with such intricate cases, but their additional modeling power is obtained at the expense of computational efficiency. For this second example, the unconstrained approach [Fig. 5(c) and (d)] clearly yields singularities in the deformation field, making holes appear in the deformed image and therefore changing the topology of the source image. The constrained method [Fig. 5(e) and (f)] produces a topology preserving result, without any hole appearing, neither during the registration process nor in the final result (see our web site http://www-ipb.u-strasbg.fr/gitim/research/index_a.html in the section on topology preserving deformable matching, for animated deformations). When the constraint increases ($J \geq 0.5$), the method is completely unable to retrieve the large displacements, since they are outside the space of feasible solutions.

As an example of application, the inter-subject registration of 2-D MR images has been considered. Inter-subject registration is a key issue in medical imaging applications involving individualized or probabilistic atlases [18], [33]. Extensive experiments with the previous unconstrained version of our deformable matching algorithm [17], have shown that the hierarchical model was able to provide accurate maps between 2-D (or 3-D) inter-subject MRI's, which shows that the modeling power of the representation is adequate in this application (in many cases of course, the mappings were not topology preserving, as expected).
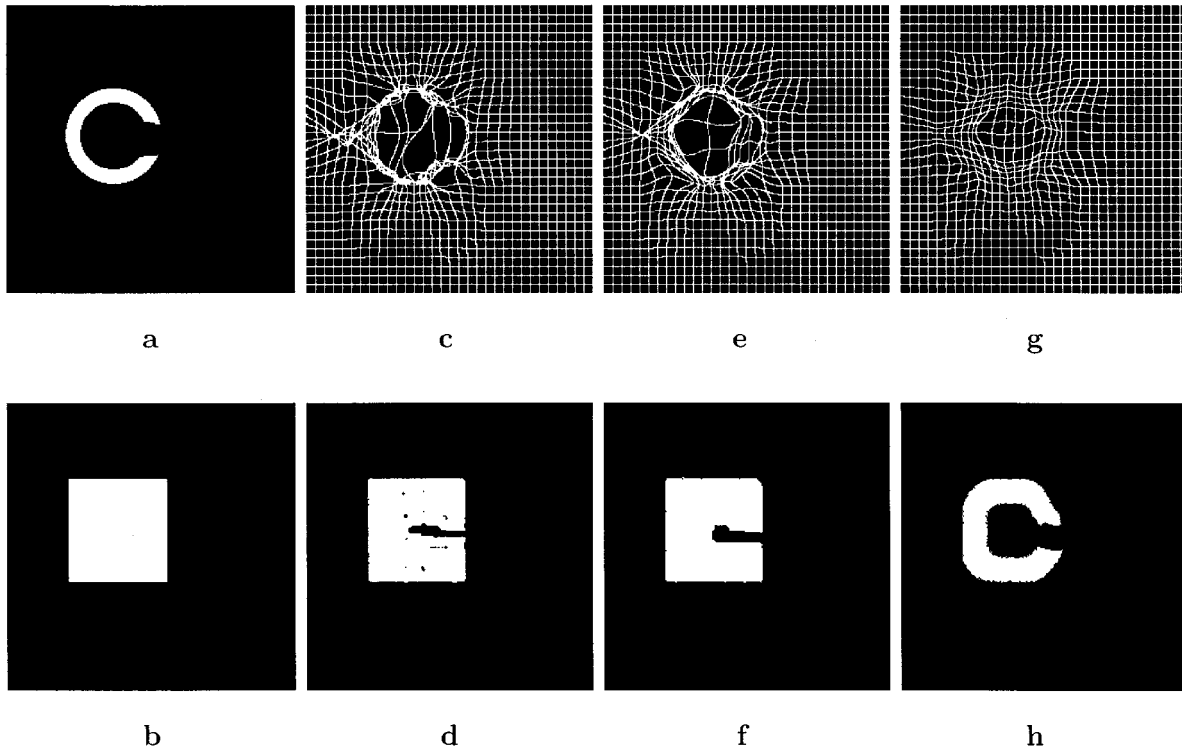
Fig. 5.   Deformable matching of (a) a capital "C" on (b) a square: (c) and (d) without any constraint; (e) and (f) with a positivity constraint $J > 0$; and (g) and (h) with the constraint $J > 0.5$.

In order to get 2-D images of two different patients, corresponding to the same part of the head, we consider two slices extracted at the same position in two 3-D MR images (256^3), after having put them in the same coordinate system, through rigid registration [34]. Fig. 6 displays the results obtained by matching the two images with different constraints. In each case, the registration was performed up to scale $L = 7$, which corresponds to exactly 32 258 parameters. The result obtained without the topology-preserving constraints [Fig. 6(d), (h), and (l)] is quite noisy, both for the deformed image and on the regular grid. When computing the Jacobian of the deformation, we notice that the local injectivity condition is violated over a large part of the image. With the constrained approach, the resulting deformation preserves topology, thus providing an anatomically coherent deformation. As the minimal value of J is increased, the deformation field becomes smoother, but the matching remains very satisfactory [see Fig. 6(g), (k), and (o)]. To illustrate the actual contribution of topology preservation, we have manually segmented the left ventricle in the source image [Fig. 7(a)]. By applying the estimated deformation on this segmentation map, we directly get a segmentation of the left ventricle in the target image. An interesting point is that a part of the left ventricle in the target image presents a contraction, reducing it to a thin line [Fig. 7(d)]. When using the unconstrained approach, the connected component formed by the source ventricle is separated into two different connected regions [Fig. 7(b)], thus modifying the topology of this structure. When the topology-preserving method is used, the structure remains connected so that the region corresponding to the thin line is well segmented [Fig. 7(c)], ensuring the anatomical coherence of the segmentation.

VI. CONCLUSION

We presented a parametric approach for topology-preserving deformable image registration. The method is based on a continuous hierarchical modeling of the deformation field, relying on the multiresolution approximation theory for finite energy signals. The deformation field is expanded on a set of scaling functions corresponding to Riesz bases of polynomial splines. These bases enable to handle topological constraints as a limited set of linear constraints on the model parameters. The method is developed in two dimensions but the 3-D extension is planned.[3] The choice of other scaling functions in 2-D and in 3-D, as well as their influence on the accuracy of the matching, is also under study.

The major contribution of the proposed constrained hierarchical approach is to enforce Jacobian positivity over the whole continuous domain Ω on which the deformable mapping is defined. Contrary to existing approaches that track discrete approximations of the Jacobian on the discrete image lattice, topology preservation is thus mathematically guaranteed over the image support, at all scales. The hierarchical estimation scheme also exhibits low sensitivity to local minima, and enables large, nonlinear deformation estimation with moderate computational burden [typical computational time for matching 256^2 images is less than 1 min on a standard single processor workstation (HP C3000 360 MHz)].

Inter-patient registration of medical images, presented in Section V, is one of the potential applications of the method. Let us

---

[3]The linearity of the Jacobian with respect to the model parameters (Appendix A) has been established for 3-D vector fields, but the linearity with respect to the spatial coordinates, is no longer verified. This issue is currently under study.
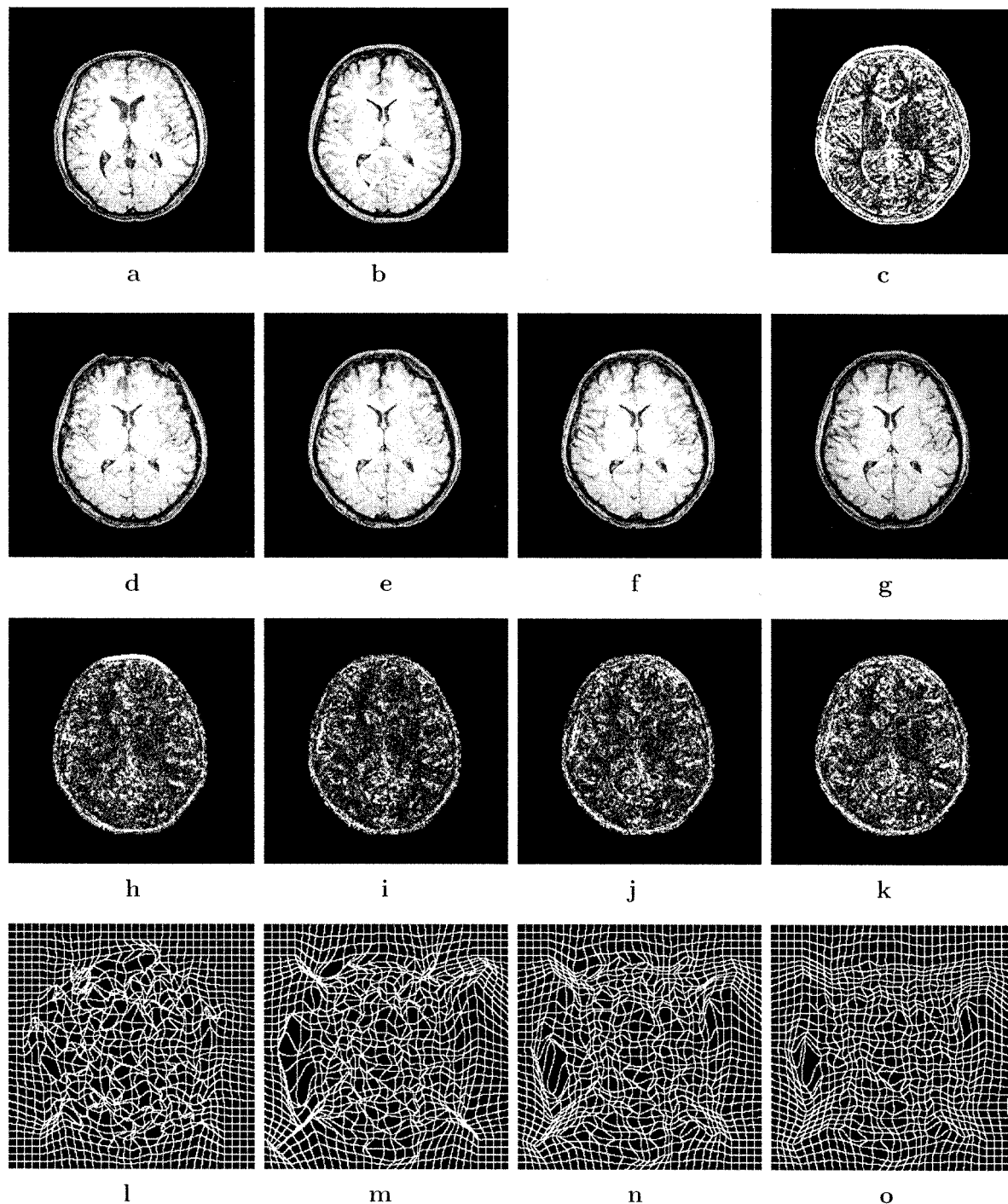
Fig. 6.   Nonrigid matching of MR images from two different individuals: (a) source (reference) image; (b) target image (patient data); (c) difference between the source and the target image; (d) result of the deformable matching without constraint; (e) result of the matching with the positivity constraint $J > 0$; (f) deformable matching with the constraint $J > 0.3$; (g) with the constraint $J > 0.5$. For each case, the difference between the deformed image and the target image is computed (h)–(k) and a superimposed regular grid of lines is also deformed to visualize the smoothness and coherence of the deformation (l)–(o).

however notice that the framework described here is also suited to many other pattern matching problems in which the topology of the underlying structures have to be preserved. In the current implementation of the method, the constraints are spatially invariant, but the method may be extended to handle spatially inhomogeneous constraints. For inter-patient registration of medical images, this represents an interesting extension since the variability in shapes among a population is not the same for all anatomical structures. A description of these variations for each structure may be very useful for instance, to perform or analyze the mapping of an atlas on a template. In other applications, one could enforce local injectivity in some part of the image while allowing singularities in other parts, in order to deal with local changes in topology.
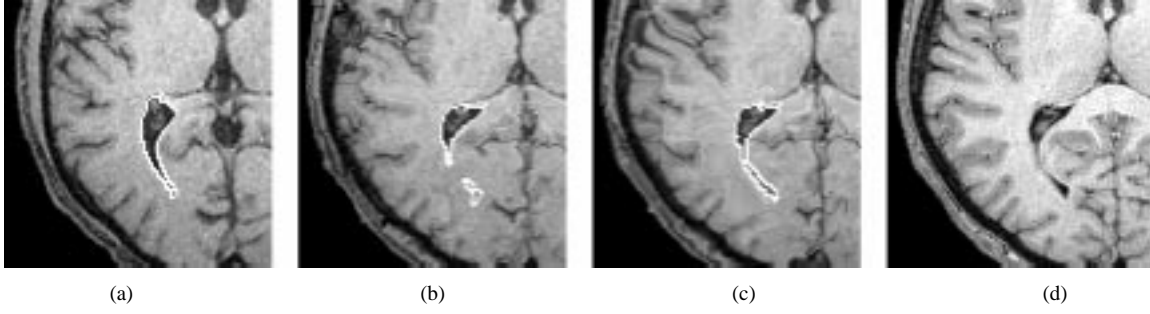
Fig. 7. Effect of the topology-preserving constraint on atlas-based segmentation using registration: (a) source image with the contour of a manual segmentation of the left ventricle superimposed (d) target image. The results of the matching of (a) on (d) are displayed: (b) using the unconstrained approached and (c) with the positivity constraint $J > 0$. By ensuring topology preservation, the constrained approach provides a connected region while the unconstrained approach separates it into two different components.

APPENDIX A
LINEARITY OF THE JACOBIAN WITH RESPECT TO THE MODEL PARAMETERS

As stated in Section IV-B, we show in this Appendix that, for an arbitrary scaling function ϕ, the Jacobian J_{h^l} of map h^l is linear with respect to the parameters $a_{x_{i,j}}^l$ and $a_{y_{i,j}}^l$.

From (5), we can write

$$\mathbf{u}^l(x,y) = \begin{cases} u_x^l(x,y) = a_{x_{i,j}}^l \phi_{i,j}^l + \tilde{u}_x^l \\ u_y^l(x,y) = a_{y_{i,j}}^l \phi_{i,j}^l + \tilde{u}_y^l \end{cases} \quad (12)$$

where $\tilde{u}_x^l = \sum_{i' \neq i} \sum_{j' \neq j} a_{x_{i',j'}}^l \phi_{i',j'}^l$ and $\tilde{u}_y^l = \sum_{i' \neq i} \sum_{j' \neq j} a_{y_{i',j'}}^l \phi_{i',j'}^l$ are the terms of u_x^l and u_y^l corresponding to the basis functions, the subscripts of which are different from (i,j). The Jacobian J_{h^l} is then given by

$$J_{h^l} = \begin{vmatrix} 1 + \frac{\partial u_x^l}{\partial x} & \frac{\partial u_x^l}{\partial y} \\ \frac{\partial u_y^l}{\partial x} & 1 + \frac{\partial u_y^l}{\partial y} \end{vmatrix}$$
$$= \alpha + \beta a_{x_{i,j}}^l + \gamma a_{y_{i,j}}^l \quad (13)$$

where

$$\alpha = 1 + \frac{\partial \tilde{u}_x^l}{\partial x} + \frac{\partial \tilde{u}_y^l}{\partial y} + \frac{\partial \tilde{u}_x^l}{\partial x}\frac{\partial \tilde{u}_y^l}{\partial y} - \frac{\partial \tilde{u}_y^l}{\partial x}\frac{\partial \tilde{u}_x^l}{\partial y}$$
$$\beta = \frac{\partial \phi_{i,j}^l}{\partial x} + \frac{\partial \phi_{i,j}^l}{\partial x}\frac{\partial \tilde{u}_y^l}{\partial y} - \frac{\partial \phi_{i,j}^l}{\partial y}\frac{\partial \tilde{u}_y^l}{\partial x}$$
$$\gamma = \frac{\partial \phi_{i,j}^l}{\partial y} + \frac{\partial \phi_{i,j}^l}{\partial y}\frac{\partial \tilde{u}_x^l}{\partial x} - \frac{\partial \phi_{i,j}^l}{\partial x}\frac{\partial \tilde{u}_x^l}{\partial y}$$

The Jacobian is therefore linear with respect to $a_{x_{i,j}}^l$ and $a_{y_{i,j}}^l$, for all $s \in \Omega$.

APPENDIX B
POSITIVITY CONSTRAINTS ON THE JACOBIAN

To enforce the positivity of the Jacobian over domain Ω, we take advantage of the linearity of J_{h^l} with respect to the spatial coordinates, in the case of the ϕ_1 scaling function.

From (6), with $d = 1$, we have

$$\phi_1(x) = \begin{cases} x+1, & \text{for } x \in [-1,0] \\ 1-x, & \text{for } x \in [0,1] \\ 0, & \text{otherwise} \end{cases} \quad (14)$$

From (3) and the parametric deformation model (5), it comes that over each square domain $S_{k,m}^l = [k/2^l, (k+1)/2^l] \times [m/2^l, (m+1)/2^l]$, $k = 0, \ldots, 2^l - 1$, $m = 0, \ldots, 2^l - 1$, the deformation field is given by (for the sake of simplification, the square domain $S_{k,m}^l$ is assumed to be $[0,1]^2$)

$$\mathbf{u}^l(x,y) = \begin{cases} u_x^l = a_{x_{k-1,m-1}}^l(1-x)(1-y) \\ \quad + a_{x_{k,m-1}}^l x(1-y) \\ \quad + a_{x_{k-1,m}}^l(1-x)y + a_{x_{k,m}}^l xy \\ u_y^l = a_{y_{k-1,m-1}}^l(1-x)(1-y) \\ \quad + a_{y_{k,m-1}}^l x(1-y) \\ \quad + a_{y_{k-1,m}}^l(1-x)y + a_{y_{k,m}}^l xy \end{cases} \quad (15)$$

The expression of the partial derivatives of $\mathbf{u}^l$ on $S_{k,m}^l$ becomes

$$\frac{\partial u_x^l}{\partial x} = \Sigma_x y - a_{x_{k-1,m-1}}^l + a_{x_{k,m-1}}^l$$
$$\frac{\partial u_x^l}{\partial y} = \Sigma_x x - a_{x_{k-1,m-1}}^l + a_{x_{k-1,m}}^l$$
$$\frac{\partial u_y^l}{\partial x} = \Sigma_y y - a_{y_{k-1,m-1}}^l + a_{y_{k,m-1}}^l$$
$$\frac{\partial u_y^l}{\partial y} = \Sigma_y x - a_{y_{k-1,m-1}}^l + a_{y_{k-1,m}}^l$$

where

$$\Sigma_x = \sum_{p=0}^{1}\sum_{q=0}^{1}(-1)^{p+q} a_{x_{k-p,m-q}}^l$$
$$\Sigma_y = \sum_{p=0}^{1}\sum_{q=0}^{1}(-1)^{p+q} a_{y_{k-p,m-q}}^l.$$

The Jacobian J is therefore given by

$$J = \lambda x + \mu y + \nu \quad (16)$$

where

$$\lambda = (1 - a_{x_{k-1,m-1}}^l + a_{x_{k,m-1}}^l)\Sigma_y$$
$$\quad + (a_{y_{k-1,m-1}}^l - a_{y_{k,m-1}}^l)\Sigma_x$$
$$\mu = (1 - a_{y_{k-1,m-1}}^l + a_{y_{k-1,m}}^l)\Sigma_x$$
$$\quad + (a_{x_{k-1,m-1}}^l - a_{x_{k-1,m}}^l)\Sigma_y$$
$$\nu = (1 - a_{x_{k-1,m-1}}^l + a_{x_{k,m-1}}^l)(1 - a_{y_{k-1,m-1}}^l + a_{y_{k-1,m}}^l)$$
$$\quad - (-a_{x_{k-1,m-1}}^l + a_{x_{k-1,m}}^l)^l(-a_{y_{k-1,m-1}}^l + a_{y_{k,m-1}}^l)$$

This expression shows that J_{h^l} is linear with respect to x and y. As a consequence, to enforce the constraint $0 < J_{\min} \leq J_{h^l}(x,y) \leq J_{\max}$ for all $x \in [0,1]^2$, we simply need to force

$0 < J_{\min} \le J_{h^l}(x,y) \le J_{\max}$ at the four "control" points $(0,0); (0,1); (1,1); (1,0)$. The values of the Jacobian at these points are

$$
\begin{aligned}
J_{h^l}(0,0) =& 1 - a_{x_{k-1,m-1}}^l + a_{x_{k,m-1}}^l - a_{y_{k-1,m-1}}^l + a_{y_{k-1,m}}^l \\
& - a_{x_{k-1,m-1}}^l a_{y_{k-1,m}}^l - a_{x_{k,m-1}}^l a_{y_{k-1,m-1}}^l \\
& + a_{x_{k,m-1}}^l a_{y_{k-1,m}}^l + a_{x_{k-1,m-1}}^l a_{y_{k,m-1}}^l \\
& + a_{x_{k-1,m}}^l a_{y_{k-1,m-1}}^l - a_{x_{k-1,m}}^l a_{y_{k,m-1}}^l \\
J_{h^l}(1,0) =& 1 - a_{x_{k-1,m-1}}^l + a_{x_{k,m-1}}^l + a_{y_{k,m-1}}^l + a_{y_{k,m}}^l \\
& - a_{x_{k,m-1}}^l a_{y_{k-1,m-1}}^l + a_{x_{k-1,m-1}}^l a_{y_{k,m-1}}^l \\
& - a_{x_{k-1,m-1}}^l a_{y_{k,m}}^l + a_{x_{k,m-1}}^l a_{y_{k,m}}^l \\
& + a_{x_{k,m}}^l a_{y_{k-1,m-1}}^l - a_{x_{k,m}}^l a_{y_{k,m-1}}^l \\
J_{h^l}(1,1) =& 1 - a_{x_{k-1,m}}^l + a_{x_{k,m}}^l - a_{y_{k,m-1}}^l + a_{y_{k,m}}^l \\
& + a_{x_{k,m}}^l a_{y_{k-1,m}}^l - a_{x_{k,m-1}}^l a_{y_{k-1,m}}^l \\
& + a_{x_{k-1,m}}^l a_{y_{k,m-1}}^l - a_{x_{k-1,m}}^l a_{y_{k,m}}^l \\
& + a_{x_{k,m-1}}^l a_{y_{k,m}}^l - a_{x_{k,m}}^l a_{y_{k,m-1}}^l \\
J_{h^l}(0,1) =& 1 - a_{x_{k-1,m}}^l + a_{x_{k,m}}^l - a_{y_{k-1,m-1}}^l + a_{y_{k-1,m}}^l \\
& + a_{x_{k,m}}^l a_{y_{k-1,m}}^l - a_{x_{k-1,m-1}}^l a_{y_{k-1,m}}^l \\
& + a_{x_{k-1,m}}^l a_{y_{k-1,m-1}}^l - a_{x_{k-1,m}}^l a_{y_{k,m}}^l \\
& + a_{x_{k-1,m-1}}^l a_{y_{k,m}}^l - a_{x_{k,m}}^l a_{y_{k-1,m-1}}^l . \quad (17)
\end{aligned}
$$

Let us now consider the optimization problem expressed in (10) or (11). The support $\Omega_{i,j}^l$ of basis function $\phi_{i,j}^l$ is simply the union of the four square domains $S_{i,j}^l, S_{i+1,j}^l, S_{i+1,j+1}^l$ and $S_{i,j+1}^l$. To enforce the constraint over $\Omega_{i,j}^l$, we therefore need 16 inequalities corresponding to the 16 control points. These inequalities derive from (17) for the four couples $(k,m) = (i,j)$, $(k,m) = (i+1,j)$, $(k,m) = (i+1,j+1)$, and $(k,m) = (i,j+1)$. The Jacobian being linear with respect to $a_{x_{i,j}}^l$ and $a_{y_{i,j}}^l$, the constraints can be expressed in matrix form as follows:

$$
0 < J_{\min} < M_{i,j}^l \begin{pmatrix} a_{x_{i,j}}^l \\ a_{y_{i,j}}^l \end{pmatrix} + b_{i,j}^l < J_{\max} \quad (18)
$$

where

$$
M_{i,j}^l =
\begin{pmatrix}
0 & 0 \\
a_{y_{i-1,j-1}}^l - a_{y_{i,j-1}}^l & 1 - a_{x_{i-1,j-1}}^l + a_{x_{i,j-1}}^l \\
1 - a_{y_{i,j-1}}^l + a_{y_{i-1,j}}^l & 1 - a_{x_{i-1,j}}^l + a_{x_{i,j-1}}^l \\
1 + a_{y_{i-1,j}}^l - a_{y_{i-1,j-1}}^l & a_{x_{i-1,j-1}}^l - a_{x_{i-1,j}}^l \\
-a_{y_{i+1,j-1}}^l + a_{y_{i,j-1}}^l & -a_{x_{i,j-1}}^l + 1 + a_{x_{i+1,j-1}}^l \\
0 & 0 \\
a_{y_{i+1,j-1}}^l - 1 - a_{y_{i+1,j}}^l & a_{x_{i+1,j}}^l - a_{x_{i+1,j-1}}^l \\
a_{y_{i,j-1}}^l - 1 - a_{y_{i+1,j}}^l & -a_{x_{i,j-1}}^l + 1 + a_{x_{i+1,j}}^l \\
a_{y_{i-1,j+1}}^l + 1 - a_{y_{i-1,j}}^l & a_{x_{i-1,j}}^l - a_{x_{i-1,j+1}}^l \\
1 - a_{y_{i-1,j}}^l + a_{y_{i,j+1}}^l & 1 - a_{x_{i,j+1}}^l + a_{x_{i-1,j}}^l \\
-a_{y_{i-1,j+1}}^l + a_{y_{i,j+1}}^l & -a_{x_{i,j+1}}^l - 1 + a_{x_{i-1,j+1}}^l \\
0 & 0 \\
a_{y_{i+1,j}}^l - 1 - a_{y_{i,j+1}}^l & -1 + a_{x_{i,j+1}}^l - a_{x_{i+1,j}}^l \\
-a_{y_{i+1,j+1}}^l - 1 + a_{y_{i+1,j}}^l & a_{x_{i+1,j+1}}^l - a_{x_{i+1,j}}^l \\
0 & 0 \\
-a_{y_{i,j+1}}^l + a_{y_{i+1,j+1}}^l & -1 + a_{x_{i,j+1}}^l - a_{x_{i+1,j+1}}^l
\end{pmatrix}
$$

and

$$
b_{i,j}^l =
\begin{pmatrix}
1 + a_{y_{i-1,j}}^l - a_{x_{i-1,j-1}}^l + a_{x_{i,j-1}}^l - a_{y_{i-1,j-1}}^l - a_{x_{i,j-1}}^l \\
\quad + a_{y_{i-1,j-1}}^l + a_{x_{i-1,j-1}}^l a_{y_{i,j-1}}^l + a_{x_{i-1,j}}^l a_{y_{i-1,j-1}}^l \\
\quad - a_{x_{i-1,j}}^l a_{y_{i,j-1}}^l + a_{x_{i,j-1}}^l a_{y_{i-1,j}}^l - a_{x_{i-1,j-1}}^l a_{y_{i-1,j}}^l \\
1 - a_{x_{i-1,j-1}}^l + a_{x_{i,j-1}}^l - a_{y_{i,j-1}}^l - a_{x_{i,j-1}}^l a_{y_{i-1,j-1}}^l \\
\quad + a_{x_{i-1,j-1}}^l a_{y_{i,j-1}}^l \\
1 - a_{x_{i-1,j}}^l + a_{x_{i-1,j}}^l a_{y_{i,j-1}}^l - a_{y_{i,j-1}}^l - a_{x_{i-1,j}}^l a_{y_{i-1,j}}^l \\
1 - a_{x_{i-1,j}}^l + a_{x_{i-1,j}}^l a_{y_{i-1,j-1}}^l - a_{y_{i-1,j-1}}^l + a_{y_{i-1,j}}^l \\
\quad - a_{x_{i-1,j-1}}^l a_{y_{i-1,j}}^l \\
1 - a_{x_{i,j-1}}^l + a_{x_{i,j-1}}^l a_{y_{i+1,j-1}}^l - a_{x_{i+1,j-1}}^l a_{y_{i,j-1}}^l \\
\quad + a_{x_{i+1,j-1}}^l - a_{y_{i,j-1}}^l \\
1 + a_{x_{i,j-1}}^l a_{y_{i+1,j-1}}^l - a_{x_{i,j-1}}^l + a_{x_{i+1,j-1}}^l - a_{y_{i+1,j-1}}^l \\
\quad + a_{y_{i+1,j}}^l - a_{x_{i+1,j-1}}^l a_{y_{i,j-1}}^l + a_{x_{i+1,j}}^l a_{y_{i,j-1}}^l \\
\quad - a_{x_{i,j-1}}^l a_{y_{i+1,j}}^l - a_{x_{i+1,j-1}}^l a_{y_{i+1,j-1}}^l \\
\quad + a_{x_{i+1,j-1}}^l a_{y_{i+1,j}}^l \\
1 + a_{x_{i+1,j}}^l + a_{y_{i+1,j}}^l - a_{y_{i+1,j-1}}^l - a_{x_{i+1,j}}^l a_{y_{i+1,j-1}}^l \\
\quad + a_{x_{i+1,j-1}}^l a_{y_{i+1,j}}^l \\
1 + a_{x_{i+1,j}}^l - a_{y_{i,j-1}}^l - a_{x_{i+1,j}}^l a_{y_{i,j-1}}^l + a_{x_{i,j-1}}^l a_{y_{i+1,j}}^l \\
1 - a_{x_{i-1,j}}^l a_{y_{i-1,j+1}}^l - a_{x_{i-1,j}}^l + a_{x_{i-1,j+1}}^l a_{y_{i-1,j}}^l \\
\quad + a_{y_{i-1,j+1}}^l - a_{y_{i-1,j}}^l \\
1 - a_{x_{i-1,j}}^l + a_{y_{i,j+1}}^l - a_{x_{i-1,j}}^l a_{y_{i,j+1}}^l + a_{x_{i,j+1}}^l a_{y_{i-1,j}}^l \\
1 - a_{x_{i-1,j+1}}^l + a_{x_{i,j+1}}^l a_{y_{i-1,j+1}}^l + a_{x_{i,j+1}}^l + a_{y_{i,j+1}}^l \\
\quad - a_{x_{i-1,j+1}}^l a_{y_{i,j+1}}^l \\
1 - a_{x_{i-1,j+1}}^l + a_{x_{i,j+1}}^l - a_{y_{i-1,j}}^l + a_{y_{i-1,j+1}}^l \\
\quad + a_{x_{i-1,j+1}}^l a_{y_{i,j+1}}^l + a_{x_{i,j+1}}^l a_{y_{i-1,j+1}}^l - a_{x_{i,j+1}}^l a_{y_{i-1,j}}^l \\
\quad - a_{x_{i-1,j+1}}^l a_{y_{i,j+1}}^l - a_{x_{i-1,j}}^l a_{y_{i-1,j+1}}^l \\
\quad + a_{x_{i-1,j+1}}^l a_{y_{i-1,j}}^l \\
1 + a_{y_{i,j+1}}^l - a_{x_{i,j+1}}^l a_{y_{i+1,j}}^l + a_{x_{i+1,j}}^l a_{y_{i,j+1}}^l + a_{x_{i+1,j}}^l \\
1 + a_{x_{i+1,j}}^l - a_{y_{i+1,j}}^l + a_{y_{i+1,j+1}}^l - a_{x_{i+1,j+1}}^l a_{y_{i+1,j}}^l \\
\quad + a_{x_{i+1,j}}^l a_{y_{i+1,j+1}}^l \\
1 - a_{x_{i+1,j}}^l a_{y_{i,j+1}}^l - a_{x_{i,j+1}}^l + a_{x_{i+1,j+1}}^l - a_{y_{i+1,j}}^l \\
\quad + a_{y_{i+1,j+1}}^l + a_{x_{i,j+1}}^l a_{y_{i+1,j}}^l + a_{x_{i+1,j+1}}^l a_{y_{i,j+1}}^l \\
\quad - a_{x_{i,j+1}}^l a_{y_{i+1,j+1}}^l - a_{x_{i+1,j+1}}^l a_{y_{i+1,j}}^l \\
\quad + a_{x_{i+1,j}}^l a_{y_{i+1,j+1}}^l \\
1 + a_{x_{i+1,j+1}}^l + a_{y_{i,j+1}}^l + a_{x_{i+1,j+1}}^l a_{y_{i,j+1}}^l - a_{x_{i,j+1}}^l \\
\quad - a_{x_{i,j+1}}^l a_{y_{i+1,j+1}}^l
\end{pmatrix}
$$

Due to the simplifying assumption that $S_{k,m}^l = [0,1]^2$, previous equations are only valid for resolution level $l = 0$. To deal with resolution 2^l it is easy to show that all terms of order $n = 0, 1, 2$, with respect to a_x^l and a_y^l, simply need to be multiplied by 2^{-nl} in (16)–(18)

APPENDIX C
LOCAL ONE-TO-ONE PROPERTY OF THE PIECEWISE C^1 DEFORMATION MAP

Theorem 2 states that the local one-to-one property, necessary to get a global homeomorphism, may be obtained, for C^1 transformations, by ensuring the positivity of the Jacobian. However, when using the ϕ_1 polynomial spline scaling function, h^l is only

a piecewise C^1 transformation (see Appendix B). We show here that this condition is sufficient to ensure the local one-to-one property of h^l.

As already established in Appendix B, with the ϕ_1 scaling function, J_{h^l} is linear with respect to x and y on each square domain $S^l_{k,m}$ (16). Let us denote $\tilde{h}^l$ the extension of $h^l(s)$, $s \in S^l_{k,m}$ to the whole $\mathbb{R}^2$ plane. The Jacobian $J_{\tilde{h}^l}$ of $\tilde{h}^l$ is linear with respect to x and y over $\mathbb{R}^2$ and strictly positive on the closed bounded set $S^l_{k,m}$. From the uniform continuity of $J_{\tilde{h}^l}$ it follows that there exists an open set S^*, containing $S^l_{k,m}$, over which $J_{\tilde{h}^l}$ is strictly positive. Applying Theorem 2 to S^*, we obtain that $\tilde{h}^l$ is locally one-to-one on S^* and then on $S^l_{k,m}$. Since $h^l = \tilde{h}^l$ on $S^l_{k,m}$, h^l is locally one-to-one on the closed bounded set $S^l_{k,m}$. However, this does not imply the local injectivity of h^l on the boundary between two square domains ($S^l_{k,m}$ and $S^l_{k+1,m}$ for instance) since the neighborhood of a point on this boundary lies simultaneously over two (or four) different squares. To address this issue, we use some elementary geometric properties related to the constrained mapping. From (15), it is easy to see that the boundaries of domain $S^l_{k,m}$ are linearly mapped to line segments. The image of the boundary of the square domain $[0,1]^2$ is thus a quadrilateral joining the following points:

$$p_1 = (a_{x\,k-1,m-1}^l, a_{y\,k-1,m-1}^l) \tag{19}$$

$$p_2 = (1 + a_{x\,k,m-1}^l, a_{y\,k,m-1}^l) \tag{20}$$

$$p_3 = (1 + a_{x\,k,m}^l, 1 + a_{y\,k,m}^l) \tag{21}$$

$$p_4 = (a_{x\,k-1,m}^l, 1 + a_{y\,k-1,m}^l) \tag{22}$$

Let $v_{i=1,\dots,3} = p_{i+1} - p_i$, $v_4 = p_1 - p_4$, denote the four vectors corresponding to the edges of the deformed square. The vector products $\det(v_i, v_{i+1})$ are nothing else but the Jacobian of h^l on the four corners of $[0,1]^2$ (17). For instance [using (16)] we have

$$
\begin{aligned}
&J_{h^l}(0,0)\\
&= \begin{vmatrix} 1 + \frac{\partial u_x^l}{\partial x}(0,0) & \frac{\partial u_x^l}{\partial y}(0,0) \\ \frac{\partial u_y^l}{\partial x}(0,0) & 1 + \frac{\partial u_y^l}{\partial y}(0,0) \end{vmatrix}\\
&- \begin{vmatrix} 1 + a_{x\,k,m-1}^l - a_{x\,k-1,m-1}^l & a_{x\,k-1,m}^l - a_{x\,k-1,m-1}^l \\ a_{y\,k,m-1}^l - a_{y\,k-1,m-1}^l & 1 + a_{y\,k-1,m}^l - a_{y\,k-1,m-1}^l \end{vmatrix}\\
&= \det(v_1, v_4).
\end{aligned}
\tag{23}
$$

The positivity constraint on the Jacobian, when applied on the four corners of each square domain $S^l_{k,m}$, thus amounts to enforcing the four angles formed by the edges of the deformed shape $h^l(S^l_{k,m})$ to remain positive. By considering domain $S^l_{k,m}$ and the eight surrounding squares, it follows that, after constrained deformation, these nine squares are transformed into a set of nine closed, bounded, simply connected and mutually disjoint regions [see Fig. 8]. Using Theorem 3, the restriction of h^l on this nine square domains is thus a global homeomorphism, which implies the desired local injectivity on the boundary of $S^l_{k,m}$. As a consequence, the positivity constraints enforced on the Jacobian ensure that transformation h^l is locally one-to-one for all the points in Ω.
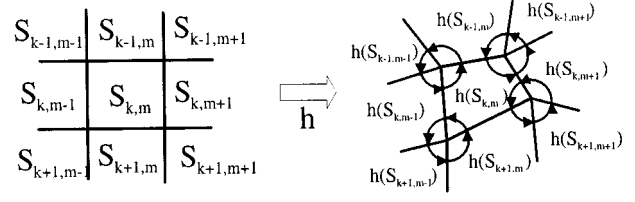

Fig. 8. Geometric properties of the parametric deformation: under the constrained approach, each square domain $S^l_{k,m}$ is deformed toward a quadrilateral, the angles of which are all positive. This property ensures local injectivity of the map even at points of discontinuous derivative.

APPENDIX D
CONSTRAINED MINIMIZATION METHOD

The linearity of the constraints enables to adapt standard constrained minimization methods. Let us consider a minimization problem under linear constraints: $\forall j \in 0, \dots, m$, $\sum_{i=1}^n c_{i,j}\theta_i + d_j > 0$, where $(\theta_i)_{i=0\dots n}$ are the n parameters to be estimated and $c_{i,j}$ and d_j are the coefficients associated to the m linear constraints to be satisfied. Given one point $\Theta = (\theta_i)_{i=0,\dots,n}$ in the feasible region (the region for which the constraints are not violated) and a direction of minimization $p = (p_i)_{i=0,\dots,n}$, we can directly compute the maximum step length α_{max}, along this direction, so that the new solution does not violate the constraints

$$\alpha_{\max} = \min_j \left(\frac{\sum_{i=1}^n c_{i,j}\theta_i + d_j}{\sum_{i=1}^n c_{i,j}p_i} \right). \tag{24}$$

Many minimization methods, with linear constraints, can be found in [29] and [30]. For our current implementation, we have used a minimization approach close to sequential linear programming [30]. The purpose is to minimize, under constraints, the local energy function (11) according to the two parameters $a_{x\,i,j}^l$ and $a_{y\,i,j}^l$ associated to basis function $\phi_{i,j}^l$. To avoid tedious iterative schemes, the problem is linearized with respect to the residual displacement, associated to a variation of the two coefficients $a_{x\,i,j}^l$ and $a_{y\,i,j}^l$. A Taylor approximation of the deformed intensity image I_2 is given by

$$
\begin{aligned}
&I_2(s + \mathbf{u}^l(s, \mathbf{A}^l) + \mathbf{u}^l(s, \delta a_{x\,i,j}^l, \delta a_{y\,i,j}^l))\\
&= I_2(s + \mathbf{u}^l(s, \mathbf{A}^l)) + \mathbf{u}^l(s, \delta a_{x\,i,j}^l, \delta a_{y\,i,j}^l)\\
&\quad \cdot \nabla I_2(s + \mathbf{u}^l(s, \mathbf{A}^l))
\end{aligned}
\tag{25}
$$

where

$$\mathbf{u}^l(s, \delta a_{x\,i,j}^l, \delta a_{y\,i,j}^l) = \begin{cases} u_x^l(s) = \delta a_{x\,i,j}^l \phi_{i,j}^l \\ u_y^l(s) = \delta a_{y\,i,j}^l \phi_{i,j}^l \end{cases}.$$

From this linearization, the two parameters $\delta a_{x\,i,j}^l$ and $\delta a_{y\,i,j}^l$ are estimated in one step by solving the corresponding least square system

$$\begin{pmatrix} \delta a_{x\,i,j}^l \\ \delta a_{y\,i,j}^l \end{pmatrix} = (M^T M)^{-1} M^T b \tag{26}$$

where

$$M = \begin{pmatrix} \nabla_x I_2(s_1)\phi_{i,j}^l(s_1) & \nabla_y I_2(s_1)\phi_{i,j}^l(s_1) \\ \vdots & \vdots \\ \nabla_x I_2(s_n)\phi_{i,j}^l(s_n) & \nabla_y I_2(s_n)\phi_{i,j}^l(s_n) \end{pmatrix}$$

$$b = \begin{pmatrix} I_2(s_1) - I_1(s_1) \\ \vdots \\ I_2(s_n) - I_1(s_n) \end{pmatrix}$$

where $\{s_1, \ldots, s_n\}$ are the n pixels in $\Omega_{i,j}$. The two parameters $\delta a_{x\,i,j}^l$ and $\delta a_{y\,i,j}^l$ can be interpreted as the search direction of the current iteration. To address the constrained minimization we then use the following scheme:

- If the new point $(a_{x\,i,j}^l + \delta a_{x\,i,j}^l, a_{y\,i,j}^l + \delta a_{y\,i,j}^l)$ is in the feasible region, this point is accepted as a new value for the two parameters $a_{x\,i,j}^l$ and $a_{y\,i,j}^l$.
- If one or more constraints are not satisfied, the maximum step length $\alpha_{\max}$ is computed using (24). The point $(a_{x\,i,j}^l + \alpha_{\max}\delta a_{x\,i,j}^l, a_{y\,i,j}^l + \alpha_{\max}\delta a_{y\,i,j}^l)$ thus obtained, lies in the feasible region.

—   If it minimizes the energy it is directly accepted.

—   If not, a 1-D minimization method (Brent's method [35]) is used to find in $[0, \alpha_{\max}]$ the step length that minimizes the energy along the direction $(\delta a_{x\,i,j}^l, \delta a_{y\,i,j}^l)$.

ACKNOWLEDGMENT

O. Musse is grateful to B. Lacolle for fruitful discussions about the mathematical issues related to topology-preserving maps.

REFERENCES

[1] J. B. A. Maintz and M. A. Viergever, "A survey of medical image registration," *Med. Image Anal.*, vol. 2, no. 1, pp. 1–36, 1998.

[2] J. C. Gee, M. Reivich, and R. Bajcsy, "Elastically deforming 3D atlas to match anatomical brain images," *J. Comput. Assist. Tomography*, vol. 17, no. 2, pp. 225–236, 1993.

[3] J.-P. Thirion, "Image matching as a diffusion process: an analogy with Maxwell's demons," *Med. Image Anal.*, vol. 2, no. 3, pp. 243–260, 1998.

[4] C. Nikou, F. Heitz, and J. P. Armspach, "Multimodal image registration using statistically constrained deformable multimodels," in *Proc. IEEE ICIP*, Chicago, IL, Oct. 4–7, 1998.

[5] M. Chen, T. Kanade, D. Pomerleau, and H. A. Rowley, "Anomaly detection through registration," *Pattern Recognit.*, vol. 32, pp. 113–128, 1999.

[6] J. Martin, A. Pentland, S. Sclaroff, and R. Kikinis, "Characterization of neuropathological shape deformations," *IEEE Trans. Pattern Anal. Machine Intell.*, vol. 20, no. 2, pp. 97–112, 1998.

[7] P. M. Thompson, D. MacDonald, M. S. Mega, C. J. Holmes, A. C. Evans, and A. W. Toga, "Detection and mapping of abnormal brain structure with a probabilistic atlas of cortical surfaces," *J. Comput. Assist. Tomography*, vol. 21, no. 4, pp. 567–581, 1997.

[8] L. Lemieux, U. C. Wieshmann, N. F. Moran, D. R. Fish, and S. D. Shorvon, "The detection and significance of subtle changes in mixed-signal brain lesions by serial MRI scan matching and spatial normalization," *Med. Image Anal.*, vol. 2, no. 3, pp. 227–242, 1998.

[9] N. C. Andreasen, R. Rajarethinam, T. Cizaldo, S. Arndt, V. W. Swayze, L. A. Flashman, D. S. O'Leary, J. C. Ehrhardt, and W. T. C. Yuh, "Automatic atlas-based volume estimation of human brain regions from MR images," *J. Comput. Assist. Tomography*, vol. 20, no. 1, pp. 98–106, 1996.

[10] G. Subsol, N. Roberts, M. Doran, J.-P. Thirion, and G. Whitehouse, "Automatic analysis of cerebral atrophy," *Magn. Reson. Imag.*, vol. 15, no. 8, pp. 917–927, 1997.

[11] T. Poggio, V. Torre, and C. Koch, "Computational vision and regularization theory," *Nature*, vol. 317, pp. 314–319, 1985.

[12] Y. Amit, "A nonlinear variational problem for image matching," *Soc. Ind. Math.*, vol. 15, no. 1, pp. 207–224, 1994.

[13] F. L. Bookstein, "Landmark methods for forms without landmarks: morphometrics of group differences in outline shape," *Med. Image Anal.*, vol. 1, no. 3, pp. 225–243, 1997.

[14] J. C. Gee, "On matching brain volumes," *Pattern Recognit.*, vol. 32, pp. 99–111, 1998.

[15] R. Szeliski and J. Coughlan, "Spline-based image registration," *Int. J. Comput. Vis.*, vol. 22, no. 3, pp. 199–218, 1997.

[16] F. L. Bookstein, "Principal warps: Thin-plate splines and the decomposition of deformation," *IEEE Trans. Pattern Anal. Machine Intell.*, vol. 11, no. 6, pp. 567–585, June 1989.

[17] O. Musse, F. Heitz, and J.-P. Armspach, "3D deformable image matching using multiscale minimization of global energy functions," in *Proc. IEEE CVPR*, vol. 2, Fort Collins, CO, 1999, pp. 478–484.

[18] G. E. Christensen, M. I. Miller, M. W. Vannier, and U. Grenander, "Individualizing neuro-anatomical atlases using a massively parallel computer," *IEEE Comput.*, pp. 32–38, 1996.

[19] G. E. Christensen, R. D. Rabbitt, and I. Miller, "Deformable templates using large deformation kinematics," *IEEE Trans. Image Processing*, vol. 5, pp. 1435–1447, Oct. 1996.

[20] A. Trouvé, "Diffeomorphisms groups and pattern matching in image analysis," *Int. J. Comput. Vis.*, vol. 28, no. 3, pp. 213–221, 1998.

[21] J. Ashburner, J. L. R. Andersson, and K. J. Friston, "High-dimensional image registration using symmetric priors," *NeuroImage*, vol. 9, pp. 619–628, 1999.

[22] R. Creighton Buck, "Advanced Calculus," in *International Series in Pure and Applied Mathematics*, 2 ed. New York: McGraw-Hill, 1965.

[23] D. L. Vallée Poussin, *Cours D'analyse Infinitésimale*, 8th ed. Paris, France: Gauthiers-Villars, 1946, vol. 1.

[24] M. P. Do Carmo, *Differential Geometry of Curves and Surfaces*. Englewood Cliffs, NJ: Prentice-Hall, 1976.

[25] G. E. Christensen, R. D. Rabbit, M. I. Miller, S. C. Joshi, U. Grenander, T. A. Coogan, and D. C. Van Essen, "Topological properties of smooth anatomic maps," in *Proc. 16th IPMI*, France, June 26–30, 1995.

[26] S. G. Mallat, "A theory for multiresolution signal decomposition: the wavelet representation," *IEEE Trans. Pattern Anal. Machine Intell.*, vol. 11, no. 7, pp. 674–693, 1989.

[27] S. Mallat, *A wavelet tour of signal processing*. New York: Academic, 1998.

[28] F. Heitz, P. Perez, and P. Bouthemy, "Multiscale minimization of global energy functions in some visual recovery problems," *Comput. Vis. Graph. Image Process.*, vol. 59, no. 1, pp. 125–134, 1994.

[29] P. E. Gill, W. Murray, and M. H. Wright, *Practical Optimization*. New York: Academic, 1981.

[30] S. S. Rao, *Engineering Optimization: Theory and Practice*, 3rd ed. New York: Wiley-Interscience, 1996.

[31] M. J. Black and A. D. Jepson, "Estimating optical flow in segmented images using variable-order parametric models with local deformations," *IEEE Trans. Pattern Anal. Machine Intell.*, vol. 18, pp. 972–986, Oct. 1996.

[32] A. Mitiche and P. Bouthemy, "Computation and analysis of image motion: a synopsis of current problems and methods," *Int. J. Comput. Vis.*, vol. 19, no. 1, pp. 29–55, 1996.

[33] P. M. Thompson, R. P. Woods, M. S. Mega ad, and A. W. Toga, "Mathematical/computational challenges in creating deformable and probabilistic atlases of the human brain," *Human Brain Mapping*, vol. 9, pp. 81–92, 2000.

[34] C. Nikou, F. Heitz, and J.-P. Armspach, "Robust voxel similarity metrics for the registration of dissimilar single and multimodal images," *Pattern Recognit.*, vol. 32, pp. 1351–1368, 1999.

[35] W. H. Press, S. A. Teukolsky, W. T. Vetterling, and B. P. Flannery, *Numerical Recipes in C. The Art of Scientific Computing*, 2nd ed. Cambridge, U.K.: Cambridge Univ. Press, 1992.

Oliver Musse received the engineer degree in physics from Ecole Nationale Superieure de Physique de Strasbourg, France, in 1997, and the Ph.D. degree from Universite Louis Pasteur, France, in 2000.

He is now teaching at Ecole Nationale Superieure de Physique, Laboratoire des Sciences de l'Image, de l'Informatique et de la Teledetection, Strasbourg (ENSPS/LSIIT). His research interests include medical image analysis, movement estimation, and deformable models.

Fabrice Heitz received the engineer degree in electrical engineering and telecommunications from Telecom Bretagne, France, in 1984, and the Ph.D. degree from Telecom Paris, France, in 1988.

From 1988 until 1994, he was with INRIA Rennes as a Senior Researcher in Image Processing and Computer Vision. He is now a Professor at Ecole Nationale Superieure de Physique, Laboratoire des Sciences de l'Image, de l'Informatique et de la Teledetection, Strasbourg, France (ENSPS/LSIIT). His research interests include statistical image modeling, image sequence analysis, and medical image analysis.

Dr. Heitz has been an Associate Editor for the IEEE TRANSACTIONS ON IMAGE PROCESSING from 1996 to 1999.

Jean-Paul Armspach received the engineering degree in 1978 from INSA Lyon, France, and the Ph.D degree from Louis Pasteur University, Strasbourg, France, in 1992.

He is currently a Research Engineer at Louis Pasteur University (IPB, UPRES-A CNRS 7004). His research interest are magnetic resonance imaging and biomedical image processing.